PHYSICAL REVIEW B **87**, 205309 (2013)

# Atomic-scale Ge diffusion in strained Si revealed by quantitative scanning transmission electron microscopy

G. Radtke,[1,2,*] L. Favre,[2] M. Couillard,[3] G. Amiard,[2] I. Berbezier,[2] and G. A. Botton[4]

[1]*IMPMC-CNRS UMR 7590, Université Pierre et Marie Curie-Paris 6, Campus Jussieu, 4 place Jussieu, F-75252 Paris Cedex 05, France*
[2]*IM2NP-UMR 7334, CNRS, Aix-Marseille Université, Faculté des Sciences de Saint-Jérôme, F-13397, Marseille, France*
[3]*Brockhouse Institute of Materials Research and Canadian Centre for Electron Microscopy, McMaster University, 1280 Main Street West, Hamilton, Ontario L8S 4M1, Canada*
[4]*Department of Materials Science and Engineering and Canadian Centre for Electron Microscopy, McMaster University, 1280 Main Street West, Hamilton, Ontario L8S 4M1, Canada*

(Received 4 February 2013; revised manuscript received 11 April 2013; published 24 May 2013)

Aberration-corrected scanning transmission electron microscopy is employed to investigate the local chemistry in the vicinity of a $Si_{0.8}Ge_{0.2}$/Si interface grown by molecular-beam epitaxy. Atomic-resolution high-angle annular dark field contrast reveals the presence of a nonuniform diffusion of Ge from the substrate into the strained Si thin film. On the basis of multislice calculations, a model is proposed to quantify the experimental contrast, showing that the Ge concentration in the thin film reaches about 4% at the interface and decreases monotonically on a typical length scale of 10 nm. Diffusion occurring during the growth process itself therefore appears as a major factor limiting the abruptness of interfaces in the Si-Ge system.

DOI: 10.1103/PhysRevB.87.205309 PACS number(s): 68.37.Ma, 61.72.uf, 68.35.Fx

## I. INTRODUCTION

To reach the next technology nodes in Si-based microelectronics, simple geometry scaling of components is no longer sufficient and alternative approaches are needed to achieve higher device performances. One of the technical challenges is to keep increasing transistor drain current, a key parameter for switching speed of electronic circuits. A first solution consists of using materials other than Si, such as GaAs or InP. However, these compounds are not easily incorporated in large manufacturing processes. A second solution, developed for complementary metal-oxide-semiconductor transistors, is based on strained Si.[1–3] In this approach, the Si channel is grown on a relaxed $Si_{1-x}Ge_x$ layer so that lattice mismatch generates strain, increasing carriers mobility in the Si layer and limiting short channel effects.[4–6]

Nanotechnologies also take advantage of stress and quantum confinement effects in two-dimensional objects, such as thin Si-Ge multilayers. For example, high-performance field effect transistors, built on a core-shell Si-Ge nanowire channel, have been obtained with intrinsic short switching delay.[7,8] This type of structure is also envisaged to improve solar cell efficiencies[9] by strain-tuning band gaps. Considering device dimensions, these systems require a perfect control of layers composition at the atomic scale as well as sharp interfaces. In many of these applications, understanding interdiffusion during growth processes will be crucial to precisely control device properties.

Many studies have been focused on Ge diffusion in relaxed Si layers to determine diffusion coefficients and activation energies.[10,11] While obtaining comparable diffusion coefficients, the results often disagree on the value of the activation energy.[12] Applying a biaxial tensile strain on the system further impacts these parameters. In pure Si layers, Ge diffuses through both vacancies and interstitial defects. Calculations predict a decrease of interstitials' formation energy with strain, while vacancies are not affected.[13] As a consequence, Ge diffusion decreases with the Si layer tensile strain, suggesting a linear dependence of activation energy on strain. However, most of these studies rely on secondary ion mass spectrometry (SIMS) technique, providing a limited depth diffusion resolution (several nanometers for high depth resolution SIMS) and no lateral diffusion information.

In this paper, we present an atomic-scale study of Ge diffusion in a strained Si layer based on aberration-corrected scanning transmission electron microscopy. The occurrence of nonuniform Ge diffusion across the interface during the growth process itself is demonstrated. These results show that this phenomenon, inherent to many fabrication processes, strongly limit the abruptness of the interface and might eventually affect the resulting device performances.

## II. EXPERIMENTAL AND COMPUTATIONAL DETAILS

A Si layer was deposited on a relaxed $Si_{0.8}Ge_{0.2}$ virtual substrate. Before introduction in the molecular beam epitaxy (MBE) setup, the substrate was chemically cleaned using a modified Shiraki procedure[14] that leaves a hydrogen terminated surface. Growth experiments were performed by MBE in a Riber system with a base pressure $p \approx 10^{-11}$ torr. A Si layer, 20 nm thick, was subsequently deposited at 450 °C to provide a perfectly clean, reproducibly flat surface and to avoid the generation of threading dislocations from the virtual substrate. The Si flux was obtained from an electron-beam evaporator and maintained constant during the growth at 0.1 monolayer $s^{-1}$. The substrate was rotated during the growth to obtain an homogeneous deposition and its temperature was monitored in real time.

In order to minimize sample preparation damage, cross-sectional transmission electron microscopy specimens were prepared by wedge mechanical polishing (with an angle of ~2°) until electron transparency in both ⟨110⟩ and ⟨100⟩ orientations. The surface was subsequently cleaned using low energy (<300 eV) Ar-ion milling for a short time (<15 min)

 ©2013 American Physical Society

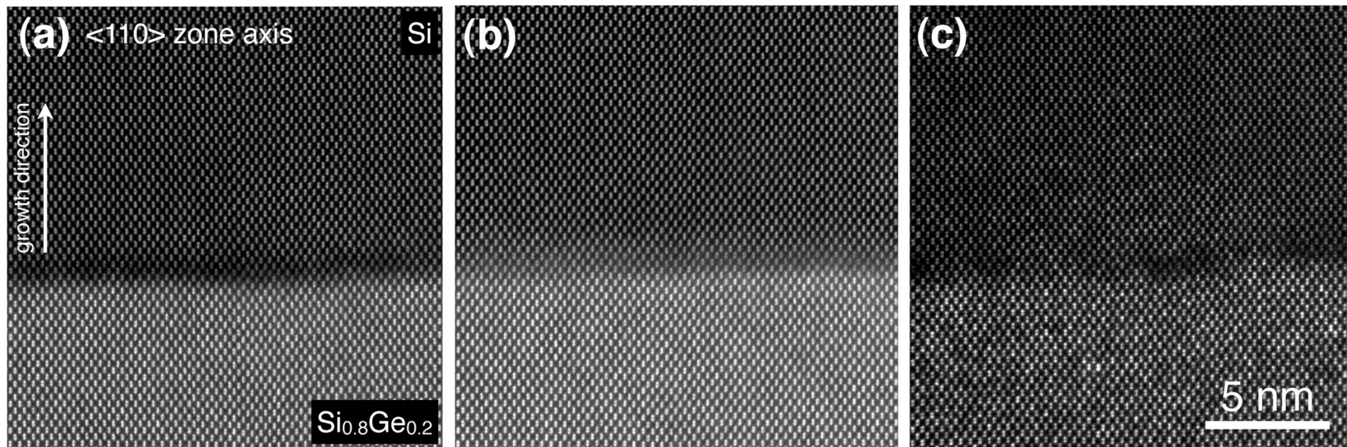


FIG. 1. (a) HAADF image (smoothed for display) of the $Si_{0.8}Ge_{0.2}$/Si interface for a thick (∼40 nm) region of the sample observed in the ⟨110⟩ zone axis. (b) LAADF image (smoothed for display) of the same region as (a). (c) HAADF image (smoothed for display) of the interface observed in a thin region (⩽15 nm) emphasizing the statistical compositional disorder in individual atomic columns of the $Si_{0.8}Ge_{0.2}$ alloy and the diffusion of Ge in the epitaxially grown Si.

before inserting the sample in the microscope. The data shown in this paper were acquired on a FEI-Titan 80-300 cubed transmission electron microscope (TEM) equipped with an aberration corrector of the probe-forming lens. For these experiments, the microscope was operated at 200 keV to reduce beam damage while preserving a good spatial resolution. The convergence semiangle was set to 18 mrad, achieving a probe size of about 0.1 nm, and the detector inner-angle to 60 mrad for high-angle annular dark field (HAADF) imaging. This angle was reduced to about 30 mrad to approach the low-angle annular dark field (LAADF) imaging conditions.

HAADF multislice image calculations have been carried out using the QSTEM simulation suite.[15] Thermal diffuse scattering has been taken into account by averaging 30 configurations and using atomic weight to approximate displacements at 300 K. A 200-keV aberration-corrected probe has been employed ($C_3 = 4\ \mu$m, $C_c = 1.4$ mm, and energy spread of 1.4 eV), a probe-forming aperture of half angle 18 mrad, an inner and an outer angle of the annular detector of 60 and 160 mrad, respectively, and a defocus $\Delta f = -5$ nm. A series of calculations have been performed on a bulk Si 3 × 3 supercell of thickness $t = 10.5$ nm observed along the ⟨100⟩ zone axis. Ge impurities have been directly substituted in the Si lattice, assuming that local structural relaxations around the impurity have a negligible effect on the resulting atomic columns intensities.

## III. RESULTS

### A. Experimental HAADF contrast

Figure 1(a) gives an overview of the $Si_{0.8}Ge_{0.2}$/Si interface observed in the ⟨110⟩ zone axis for a thick part of the specimen ($t \sim 40$ nm). A largely homogeneous contrast, free from any substantial intensity fluctuations of the individual atomic columns, is observed on both sides of the interface, either on the brighter $Si_{0.8}Ge_{0.2}$ substrate or on the darker Si layer. Interestingly, these two regions are separated by a darker band of about 2 nm thickness running along the interface. An image of the same area [see Fig. 1(b)] was recorded under the same conditions using a lower inner angle of the ADF detector—these conditions approaching what has previously been called LAADF—and exhibits, on the contrary, a reinforced intensity in the interfacial region. These intensity variations are typically associated with the presence of strain-induced dechannelling in thick specimens.[16] The observation of thinner areas of the specimen in HAADF also confirms the presence of this darker band localized at the interface, as shown in Fig. 1(c).

As this effect is likely to arise from a partial relaxation associated with the thinning procedure of the specimen inherent to transmission electron microscopy, two-dimensional (2D) finite element modeling (FEM) has been carried out in the framework of anisotropic elasticity. In the absence of plastic relaxation, the original state of the sample, supposedly infinite in the $xy$ plane, corresponds to a biaxially stressed Si layer deposited on the (001) surface of the $Si_{0.8}Ge_{0.2}$ substrate. The lattice parameters and elastic coefficients employed in the following are respectively $a_{\mathrm{Si}} = 5.431$ Å, $C_{11} = 165.8$ GPa, $C_{12} = 63.9$ GPa, and $C_{44} = 79.6$ GPa for the Si film, and $a_{\mathrm{SiGe}} = 5.472$ Å, $C_{11} = 158.3$ GPa, $C_{12} = 60.8$ GPa, and $C_{44} = 77.0$ GPa for the $Si_{0.8}Ge_{0.2}$ substrate.[17,18] The theoretical in-plane components of strain in the thin film are $\epsilon_{xx} = \epsilon_{yy} = 7.5 \times 10^{-3}$ corresponding to high tensile in-plane components of stress $\sigma_{xx} = \sigma_{yy} = 1.35$ GPa whereas the out-of-plane component of strain is $\epsilon_{zz} = -5.8 \times 10^{-3}$. Starting from this initial configuration, the effect of thinning of the TEM foil has been evaluated numerically by 2D FEM. In the results presented hereafter, the $x$ direction is taken as the ⟨110⟩ thinning direction, or beam propagation direction, $z$ is the growth direction, and $y$ is the other ⟨110⟩ direction along which the sample is supposed infinite. As the angle employed when polishing the TEM specimen was relatively low (∼2°), the wedge shape of the sample is not taken into account in this model. Calculated displacements along $x$ and $z$ for a sample of thickness $t_x = 10$ nm, i.e., corresponding to the experimental case of Fig. 1(c), are shown in Fig. 2(a) for the region localized close to the interface whereas the global geometry of the specimen is presented in Fig. 2(b). It is particularly

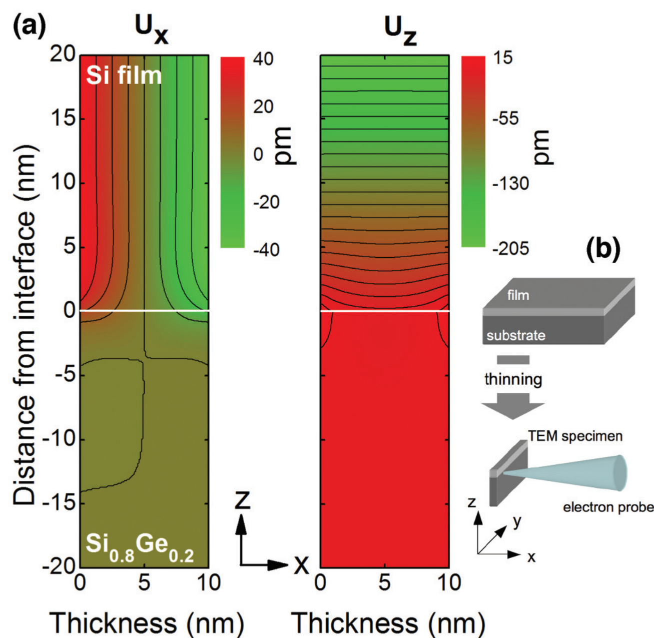


FIG. 2. (Color online) (a) Cross-section view of the displacements calculated by 2D FEM for a sample of thickness 10 nm. A bending of the atomic planes of maximum amplitude of ∼0.1 Å in the direction ($z$) perpendicular to the beam propagation direction ($x$) is expected in a region localized within a few nanometers from the interface. (b) Geometry of the transmission electron microscopy specimen.

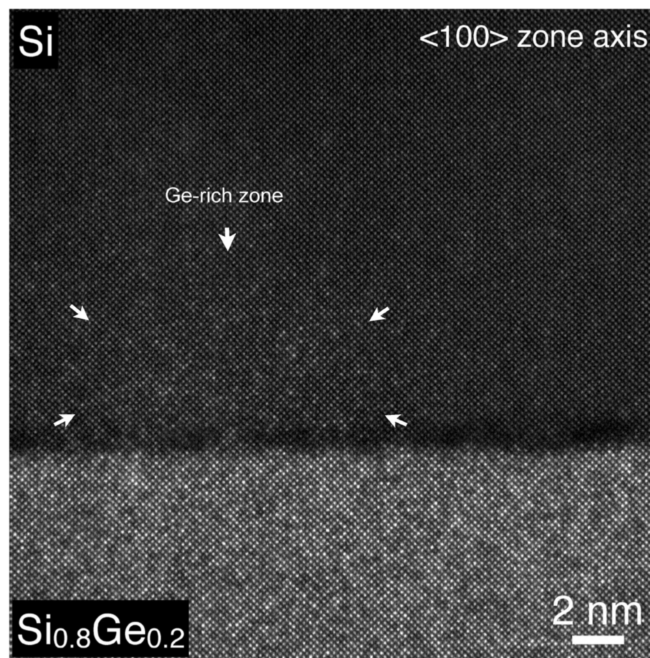


FIG. 3. HAADF image (smoothed for display) of the $Si_{0.8}Ge_{0.2}$/Si interface for a thin (∼11 nm) region of the TEM sample observed in the ⟨100⟩ zone axis. Ge-rich region in the Si layer is delimited by arrows.

interesting to note here that relaxation associated with the thinning induces inhomogeneous displacements within the thickness of the TEM sample for both $x$ and $z$ directions. More specifically, the $U_z$ component induces a bending of the atomic planes in a region localized close to the interface with a maximum amplitude estimated to about 0.1 Å (as measured between the top or bottom surfaces and the $xy$ plane located at half the thickness of the TEM specimen). The dark band observed systematically in the interfacial region (∼2 nm thickness) in HAADF might therefore be attributed to the partial dechannelling associated to this local deviation from perfectly aligned atoms in the columns, consistent with previous studies,[19,20] and appears as an unavoidable artefact associated to the TEM sample preparation in strained samples.

However, Fig. 1(c) reveals additional characteristics of the sample. First, large fluctuations of the atomic column intensities are observed in the area corresponding to the $Si_{0.8}Ge_{0.2}$ substrate. These fluctuations, representative of the local compositional disorder expected for a $Si_{0.8}Ge_{0.2}$ alloy, are strongly enhanced by the reduced thickness of the sample in Fig. 1(c) whereas they are largely averaged out for thicker areas, as shown in Fig. 1(a). Second, the diffusion of Ge atoms in the epitaxial Si thin film, not visible in thicker areas of the specimen, can be clearly identified and appear under the form of brighter atomic columns in the Si lattice. The Ge impurity distribution is characterized by a maximum concentration localized close to the interface and gradually decaying when moving away from the substrate. Unexpectedly, the lateral Ge diffusion distribution is nonuniform and exhibits fluctuations on a typical length scale of 10 nm when moving along the interface. This effect can be clearly visualized in Fig. 3, showing an HAADF image of the sample recorded along the ⟨100⟩ zone axis and where the Ge diffusion in Si appears stronger in the left part than in the right part of the image. As the strong 111 reflections are not excited in this zone axis, a better contrast of the Ge atoms is expected for this orientation compared to the ⟨110⟩ zone axis.[21]

### B. Multislice calculations

Quantification of the contrast in our present study appears as a relatively delicate task by comparison to other systems involving much heavier impurities in semiconductor matrices and where steplike intensity variations can be directly correlated to the number of impurities present in the atomic columns.[22,23] Although the intensity scattered at high angles by an isolated atom roughly scales as $Z^{1.7}$,[24] meaning that a Ge atom scatters four times more than a Si atom, the presence of Ge as substitutional impurities in the Si crystalline matrix strongly weakens their visibility. In particular, channelling of the fast electrons by the host crystal makes the scattered intensity dependent on both the local thickness and the depth of the impurity in the host atomic column. In order to estimate the atomic column intensity increase associated with the presence of a substitutional Ge impurity with respect to the intensity of a (pure Si) reference column, frozen phonon multislice simulations have been carried out. A series of calculations have been performed on bulk Si of thickness $t = 10.5$ nm observed along the ⟨100⟩ zone axis with a single Ge substitutional impurity located at different depths.

The results, presenting the intensity increase of the Ge-containing column as a function of its depth position, are shown in Fig. 4(a). A large variation of the intensity is found,

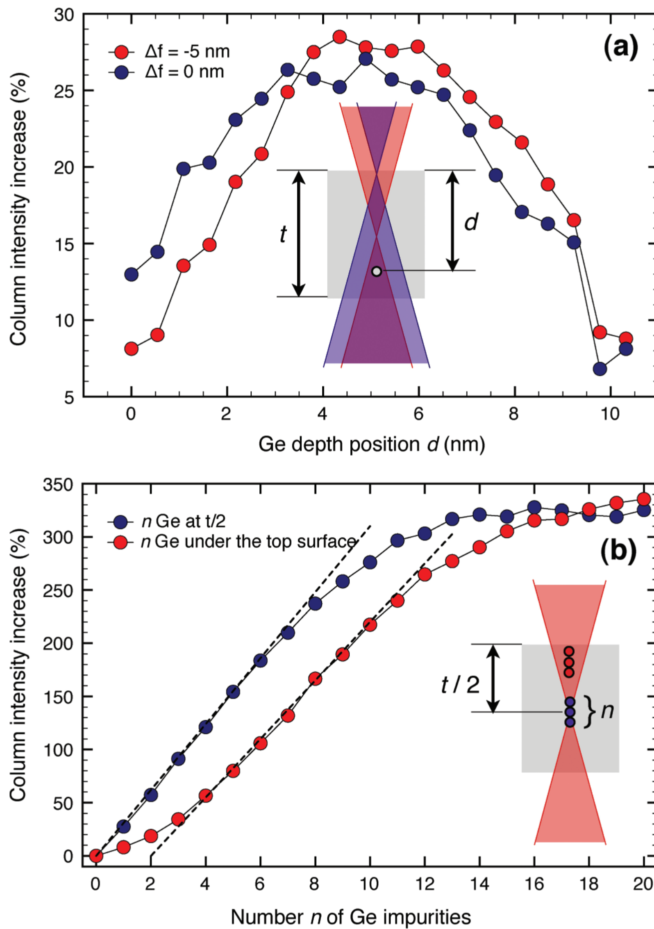


FIG. 4. (Color online) (a) Calculated intensity increase of the Ge containing atomic column as a function of the impurity depth position $d$ for $\Delta f = -5$ and 0 nm. (b) Intensity increase of the Ge containing atomic column as a function of the number $n$ of adjacent impurities located around half the thickness of the specimen or under the top surface of the sample. The defocus is kept constant here and fixed to $\Delta f = -5$ nm.

from about 8% increase when the impurity is located close to the top or bottom surface of the specimen to about 29% for an impurity located close to half the thickness of the specimen, i.e., when the electron probe is focused close to the plane containing the substitutional impurity. The average intensity increase for a single Ge impurity in a 10.5-nm-thick Si crystal observed along the ⟨100⟩ zone axis is therefore close to 20%. Additional calculations performed under the same conditions but with a defocus $\Delta f = 0$ nm, i.e., for a probe focussed at the top surface of the sample, are also shown in Fig. 4(a). The observed intensity variation displays a similar behavior with, however, a slight asymmetry reinforcing the intensity of impurities located at lower depth and weakening that of deeper impurities. The average intensity increase of a single Ge impurity remains close to 20% and therefore appears to be relatively independent from the precise defocus value actually employed in the experiments.

A second series of calculations, shown in Fig. 4(b), have been carried out for a sample containing an increasing number of adjacent Ge impurities in the same atomic column and centered around half the sample thickness in depth. The defocus is kept constant here and fixed to $\Delta f = -5$ nm. Under these conditions, a clear proportionality of the column intensity with the number of Ge impurities is observed for $1 \leqslant n \leqslant 8$ Ge impurities. When this number is further increased, a deviation from the linear regime takes place and a saturation arises for about 13 Ge atoms. Similar calculations have been carried out in the unfavorable case where the Ge impurities are located under the top surface of the sample while the defocus is maintained to $\Delta f = -5$ nm. In such a configuration, the linear intensity increase with the number of impurities is still present but shifted to the $3 \leqslant n \leqslant 11$ range. These results show that the assumption of a linear increase of the intensity with the number of substitutional Ge is only verified under certain conditions of defocus and depth positioning of the impurities and up to a maximum number of about 10 impurities, i.e., as long as the number of Ge is less than half the total number of atoms in the column.

Although the number of potential configurations to consider when two or more impurities are present in the same atomic column brings a systematic study of the impact of their depth position on the column intensities out of the scope of this paper, a subset of configurations (not shown here) involving two to ten impurities have been considered. The main conclusions resulting from this study are (i) depending on the impurities depth positions, a column containing $n$ Ge atoms can display a higher intensity than a column containing $n + 1$ Ge atoms; (ii) when $n \geqslant 3$, this observation can be extended, and a column containing $n$ Ge can display a higher intensity than a column containing $n + 1$ or $n + 2$ Ge atoms. These general conclusions are clearly illustrated in Fig. 4(b) in the particular case of clustered impurities located either in the middle or at the top surface of the sample.

### C. Model

On the basis of the results of the multislice calculations shown above, a quantitative analysis of the experimental data has been carried out. A proper extraction of the HAADF atomic column intensities shown in Fig. 3 can be obtained by optimizing an expectation model on the raw experimental data (HAADF images have been smoothed here only for display). In this work, the HAADF contrast has been modelled as a sum of 2D Gaussians superposed to a constant background:[21,25]

$$I_{\text{tot}} = I_0 + \sum_{i=1}^{N} \alpha_i \exp\left(-\frac{(x - x_i)^2 + (y - y_i)^2}{2\sigma^2}\right), \quad (1)$$

where $I_0$ is the background intensity, $N$ is the number of atomic columns in the image, $\alpha_i$ is the amplitude of the Gaussian located at position $(x_i, y_i)$. During the optimization procedure, based on the Levenberg-Marquardt algorithm, the full width at half maximum of the Gaussians is kept fixed (it was adjusted in the Ge-free area on the thin film) and the background is evaluated locally on areas of about $2 \times 2$ nm$^2$ to account for long-range thickness variations over the large area analyzed (of about $25 \times 25$ nm$^2$). A typical result of this procedure performed on the $Si_{0.8}Ge_{0.2}$ substrate is presented in Fig. 5, where the raw HAADF image is shown in (a) and the optimized model in (b). A line profile, integrated over five pixels, is also shown in Fig. 5(c), demonstrating the excellent agreement

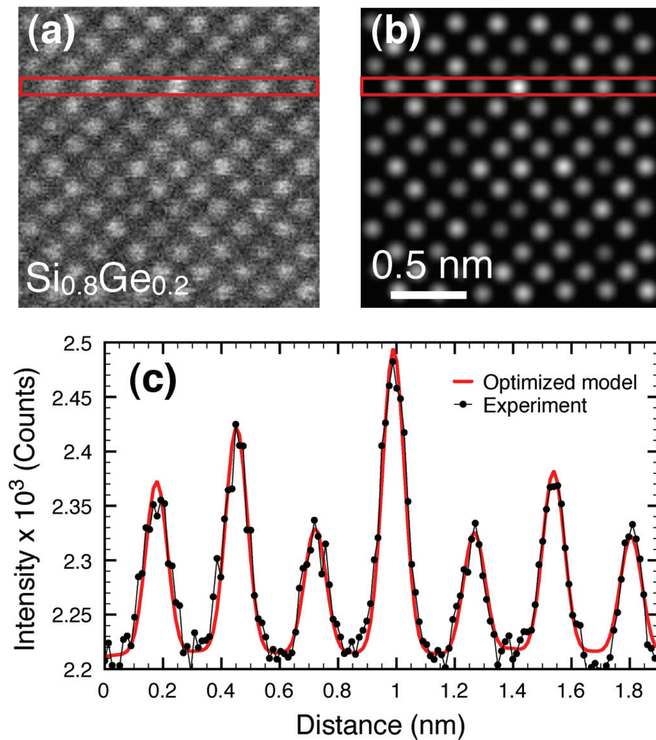


FIG. 5. (Color online) (a) Typical row experimental HAADF image recorded in a thin region of the $Si_{0.8}Ge_{0.2}$ substrate. (b) Refined model of image (a). (c) Line profile through an atomic row integrated over five pixels comparing experimental and modelled intensities.

obtained between experimental and modelled images. The atomic column intensities are then simply extracted as the volume under the optimized Gaussians.

The normalized intensities of 1274 atomic columns for a region located at about 16 nm from the interface in the Si thin film (i.e., on the very top of Fig. 3) are presented in Fig. 6(a) under the form of a histogram. Interestingly this histogram, corresponding to a region which can be considered as Ge free in first approximation, exhibits a non-negligible width. A good Gaussian fit, also shown in the figure, is obtained with a standard deviation $\sigma = 0.12$. This result, illustrating the fact that a substantial intensity distribution is observed in HAADF imaging even for a set of supposedly identical atomic columns (the most obvious case is that of the bulk, impurity-free sample) has already been reported in different studies[21,26,27] and might be induced by local thickness variations, surface damage associated with sample preparation, residual instrumental instabilities, or experimental detection noise. The presence of this experimental intensity distribution, expected to be of the same order of magnitude in areas containing Ge impurities, therefore results in the impossibility of attributing a precise origin to the intensity increase of a specific atomic column. In order to circumvent this difficulty, we based our analysis of the experimental intensities on a statistical approach. Averaging out the compositional heterogeneities observed along the interface, similar histograms, based on the analysis of areas containing 1274 columns and located at different distances from the interface [symbolized by the rectangles in the insets of Figs. 6(a)–6(h)], have been constructed.

The evolution of these histograms, when moving toward the interface, is characterized by a progressive and asymmetric broadening with an extended tail on the high intensity side of the distribution. Modeling of these intensity histograms has been carried out on the basis of the following simplifying assumptions:

(i) *Ge impurities are locally randomly distributed in the Si matrix (this is also supposed to be valid in the $Si_{0.8}Ge_{0.2}$ substrate).* This assumption implies that the probability for an individual column of $N$ atoms located in a region of nominal composition $C$ to contain $n$ Ge impurities follows a binomial distribution:[27,28]

$$P_{N,C}(n) = \frac{N!}{n!(N-n)!} C^n (1-C)^{N-n}. \quad (2)$$

(ii) *The average intensity of a column containing a single Ge impurity is 20% higher than the intensity of a reference (pure Si) column.* As shown by multislice calculations, this average value is quite robust and fairly independent (within a range of a few nanometers) from the precise defocus employed in the experiments. However, the intensity distribution induced by the depth position of the impurity should also be taken into account, as discussed below.

(iii) *The average HAADF intensity of an atomic column increases linearly with the number of impurities present in the column.* This assumption is only verified in multislice calculations under specific conditions of defocus and depth positioning of the impurities. Therefore, extending the remark of assumption (ii), an intensity distribution is also expected when $n > 1$ impurities are present in the same column.

(iv) *All atomic columns are characterized by an intrinsic experimental intensity distribution, independently from their composition.* As discussed above, this distribution is primarily associated to experimental factors and accounted for by a Gaussian distribution of standard deviation $\sigma = 0.12$ measured on the Si (close to impurity-free) film [see Fig. 6(a)]. Interestingly, this experimental distribution is relatively large and might also account approximately for the intensity distribution associated with the depth position of the impurities mentioned in assumptions (ii) and (iii). Indeed, as can be seen in Fig. 6, the Gaussians employed in this model to account for the intensity distribution of $n$, $n+1$, and $n+2$ Ge containing columns exhibit significant overlaps, consistent with the conclusions drawn from multislice calculations.

Extraction of the local concentration is based on the following procedure. A set of Gaussians of fixed widths [assumption (iv)] and fixed mean values [assumptions (ii) and (iii)] is defined. Their relative intensities are fixed by the binomial distribution [assumption(i)] for a given thickness of the sample and a given local concentration. When the sample thickness is known, impurity concentration is the only unknown that remains to be determined by optimizing the model on the experimental histogram.

Results of this optimization procedure for the different areas of the sample are shown in Figs. 6(b)–6(h). Individual Gaussians employed to construct this model and representing the relative proportion of columns containing 0, 1, 2, ....

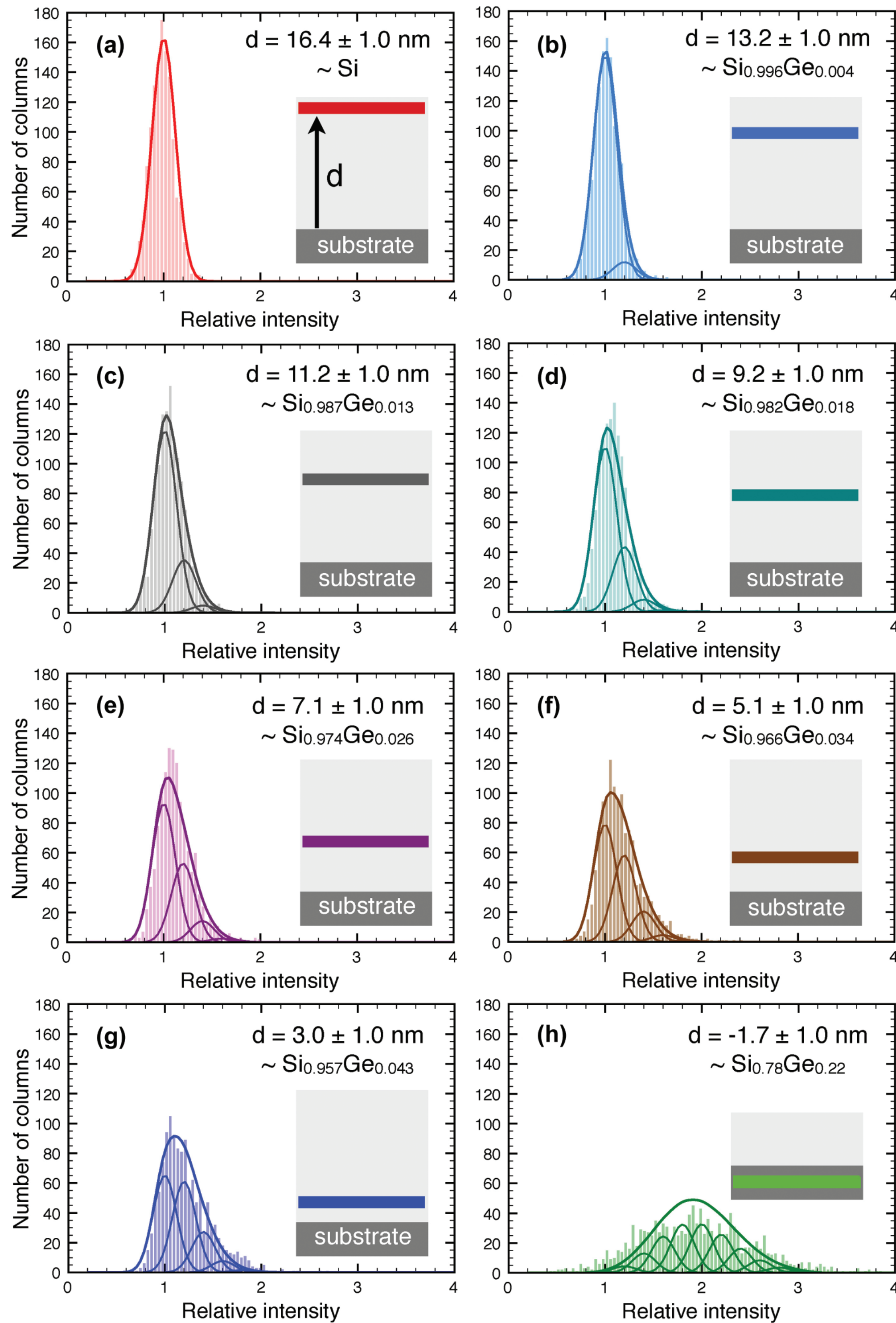


FIG. 6. (Color online) (a)–(h) Histograms of atomic column intensities as a function of the distance from the interface. Each histogram is built from the analysis of 1274 atomic columns. A model assuming a random distribution of the Ge impurities and based on a binomial distribution is shown in each case. Histogram (a) corresponds to the reference of impurity-free Si.

Ge atoms are also shown. The Ge concentration profile in the interfacial region is shown in Fig. 7. Measurement of the local thickness based on electron energy-loss spectroscopy in the area shown in Fig. 3 has been performed using the log-ratio method and a total inelastic mean free path for crystalline Si at 200 keV of $\lambda_i = 145$ nm.[29] An absolute thickness of about 11 nm has been obtained. However, as this method might be inaccurate for very thin samples, vertical error bars representing the effect of a variation of $\pm 2$ nm in the thickness on the extracted local composition are shown in

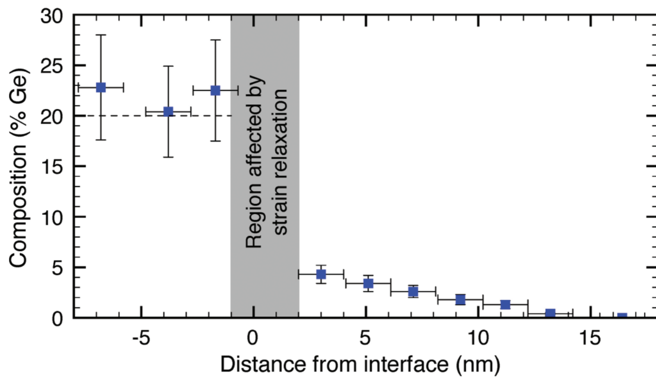


FIG. 7. (Color online) Ge composition profile obtained from the statistical analysis of the HAADF intensities of Fig. 3. Horizontal and vertical error bars correspond respectively to the width of the areas analyzed (2 nm) and to the composition variation associated to an error of 11 ± 2 nm on the measured thickness of the sample.

Fig. 7. They have been obtained by applying the optimization procedure presented above assuming a local thickness of 9 and 13 nm, respectively. Horizontal error bars give the width of the area analyzed to construct the experimental histograms (2 nm). The profile obtained on the thin film shows an almost linearly decreasing Ge concentration from a maximum of about 4% at 3 nm from the interface to below 0.4% at 13 nm. In spite of the different assumptions on which this model has been constructed, analysis of the histograms obtained on the substrate lead to an estimated composition of the alloy close (within a few percent) to its nominal composition of 20%. However, it should be added here that a straightforward application of this approach to $Si_{0.8}Ge_{0.2}$ might be hindered by static atomic displacements generated by the difference of atomic radii between Si and Ge. These local deviations from the atomic sites of the average crystalline lattice of the alloy might indeed have a stronger effect on the HAADF contrast in $Si_{0.8}Ge_{0.2}$(Refs. 30 and 31) than in the Si film (due to its low Ge concentration). These atomic displacements have not been taken into account in our multislice calculations.

## IV. DISCUSSION

Our results clearly show the occurrence of Ge diffusion from the $Si_{0.8}Ge_{0.2}$ substrate into the biaxially strained Si thin layer over a typical length scale of about 10 nm. These atomic-scale observations also reveal that this diffusion process is largely nonuniform along the interface and characterized by an alternation of Ge-rich and Ge-poor zones extending over areas of the same size (typically 10 nm). The occurrence of intermixing during the growth process itself has already been pointed out as a major factor limiting the abruptness of interfaces in Ge-Si systems.[32,33]

Based on the data published by Zangenberg and coworkers,[11] the extrapolated diffusion coefficient of Ge in relaxed Si at 450 °C would be $D = 1.2 \times 10^{-30}$ cm$^2$ s$^{-1}$ and the corresponding characteristic diffusion length $2\sqrt{Dt}$ would therefore be negligible. It should be added here that tensile strain in the Si thin film would further weaken this process. A composition gradient-driven diffusion process is therefore very unlikely to explain our observations.

Besides the compositional gradient created at the interface after starting the growth of the thin film, other microscopic mechanisms can be at the origin of this phenomenon. The lower surface energy of Ge compared to Si (Ref. 34) [estimated to 1835 and 2130 mJ/m$^2$, respectively, for a (100) surface] might induce the formation of a Ge-rich surfactant layer during the growth process by exchange of Si atoms of the topmost layer with underlying Ge atoms from the substrate. Such a process would lead to a progressively decreasing Ge concentration as the Si layer thickness increases, as observed experimentally. This surfactant effect is also suspected to occur in other semiconductor-semiconductor systems.[35] This process, favoring intermixing at the interface, would further participate in the minimization of strain energy, as it tends to reduce the lattice mismatch between the substrate and the thin film in the absence of plastic relaxation. Both phenomena are certainly very sensitive to the original surface state of the substrate and nanometer-scale surface composition variations or structural defects, such as atomic steps, might be at the origin of the heterogeneities of the Ge diffusion observed along the interface and of the non-Fickian Ge profile extracted from these observations.

## V. CONCLUSION

In this paper, we have presented an atomic-scale investigation of the local chemistry in the vicinity of a $Si_{0.8}Ge_{0.2}$/Si interface grown by MBE based on quantitative aberration-corrected scanning transmission electron microscopy. These results demonstrate the ability of HAADF imaging to characterize the diffusion of Ge impurities in a strained Si thin film. Despite the fact that the relatively low $Z$ of Ge greatly hinders its visibility in the Si matrix and prevents a column-by-column analysis of the impurity concentration under our experimental conditions, we have shown that a nanometer-scale characterization of the diffusion process can nonetheless be obtained. At the atomic scale, Ge distribution in the thin film appears to be essentially nonuniform along the interface. When averaging out these heterogeneities, a concentration of about 4% close to the interface and decreasing monotonically on a typical length scale of 10 nm can be retrieved from a statistical analysis of the experimental images. This diffusion process takes place during the growth and is certainly strongly affected by surface segregation and strain. Its occurrence appears therefore as a major factor limiting the abruptness of interfaces as well as the composition control of epitaxially grown thin layers in Si-Ge based nanostructures.

## ACKNOWLEDGMENTS

The authors are indebted to A. Ronda in charge of the NanoTecMat Platform (IM2NP, Marseille), where MBE experiments were carried out. Electron microscopy was carried out at the Canadian Centre for Electron Microscopy, a facility supported by the NSERC (Canada) and McMaster University. G.R. and G.A.B. acknowledge the Fonds France-Canada pour la Recherche for partial support of this collaboration. G.A.B is also grateful to NSERC for supporting this experimental work via a Discovery grant.

*guillaume.radtke@impmc.upmc.fr


[1] R. A. Donaton, D. Chidambarrao, J. Johnson, P. Chang, Y. Liu, W. K. Henson, J. Holt, X. Li, J. Li, A. Domenicucci, A. Madan, K. Rim, and C. Wann, in *Conference on Electron Devices Meeting, IEDM'06* (IEEE, Piscataway, NJ, 2006), pp. 465–468.

[2] K.-W. Ang, C.-H. Tung, N. Balasubramanian, G. S. Samudra, and Y.-C. Yeo, IEEE Electron Device Lett. **28**, 609 (2007).

[3] K.-W. Ang, J. Lin, C.-H. Tung, N. Balasubramanian, G. S. Samudra, and Y.-C. Yeo, IEEE Trans. Electron Devices **55**, 850 (2008).

[4] D. J. Paul, Semicond. Sci. Technol. **19**, R75 (2004).

[5] F. Capasso, Science **235**, 172 (1987).

[6] F. Schäffler, Semicond. Sci. Technol. **12**, 1515 (1997).

[7] L. J. Lauhon, M. S. Gudiksen, D. Wang, and C. M. Lieber, Nature (London) **420**, 57 (2002).

[8] J. Xiang, W. Lu, Y. Hu, Y. Wu, H. Yan, and C. M. Lieber, Nature (London) **441**, 489 (2006).

[9] M. D. Kelzenberg, S. W. Boettcher, J. A. Petykiewicz, D. B. Turner-Evans, M. C. Putnam, E. L. Warren, J. M. Spurgeon, R. M. Briggs, N. S. Lewis, and H. A. Atwater, Nat. Mater. **9**, 239 (2010).

[10] N. E. B. Cowern, P. C. Zalm, P. van der Sluis, D. J. Gravesteijn, and W. B. de Boer, Phys. Rev. Lett. **72**, 2585 (1994).

[11] N. R. Zangenberg, J. Lundsgaard Hansen, J. Fage-Pedersen, and A. Nylandsted Larsen, Phys. Rev. Lett. **87**, 125901 (2001).

[12] P. Fahey, S. S. Iyer, and G. J. Scilla, Appl. Phys. Lett. **54**, 843 (1989).

[13] A. Antonelli and J. Bernholc, MRS Proc. **163**, 609 (1989).

[14] A. Ishizaka and Y. Shiraki, J. Electrochem. Soc. **133**, 666 (1986).

[15] C. Koch, Ph.D. thesis, Arizona State University, 2002.

[16] Z. Yu, D. A. Muller, and J. Silcox, J. Appl. Phys. **95**, 3362 (2004).

[17] J. P. Dismukes, L. Ekstrom, and R. J. Paff, J. Phys. Chem. **68**, 3021 (1964).

[18] F. Schäffler, in *Properties of Advanced Semiconductor Materials GaN, AlN, InN, BN, SiC, SiGe*, edited by M. E. Levinshtein, S. L. Rumyantsev, and M. S. Shur (John Wiley & Sons, New York, 2001), pp. 149–188.

[19] X. Wu, M. D. Robertson, M. Kawasaki, and J.-M. Baribeau, Ultramicroscopy **114**, 46 (2012).

[20] V. Grillo, Ultramicroscopy **109**, 1453 (2009).

[21] Y. Oshima, Y. Hashimoto, Y. Tanishiro, K. Takayanagi, H. Sawada, T. Kaneyama, Y. Kondo, N. Hashikawa, and K. Asayama, Phys. Rev. B **81**, 035317 (2010).

[22] M. Couillard and G. Radtke, A. P. Knights and G. A. Botton Phys. Rev. Lett. **107**, 186104 (2011).

[23] H. Okuno, J.-L. Rouvière, P.-H. Jouneau, P. Bayle-Guillemaud, and B. Daudin, Appl. Phys. Lett. **96**, 251908 (2010).

[24] E. J. Kirkland, in *Advanced Computing in Electron Microscopy* (Plenum Press, New York, 1998), p. 93.

[25] S. Van Aert, J. Verbeeck, R. Erni, S. Bals, M. Luysberg, D. Van Dick, and G. Van Tendeloo, Ultramicroscopy **109**, 1236 (2009).

[26] S. Van Aert, K. J. Batenburg, M. D. Rossell, and G. Van Tendeloo, Nature (London) **470**, 374 (2011).

[27] P. M. Voyles, D. A. Muller, J. L. Grazul, P. H. Citrin, and H.-J. L. Gossmann, Nature (London) **416**, 826 (2002).

[28] J. M. Pénisson, Ultramicroscopy **51**, 264 (1993).

[29] R. F. Egerton, in *Electron Energy-Loss Spectroscopy in the Electron Microscope*, 3rd ed. (Springer, New York, 2011), p. 420.

[30] V. Grillo, E. Carlino, and F. Glas, Phys. Rev. B **77**, 054103 (2008).

[31] A. Rosenauer, T. Mehrtens, K. Müller, K. Gries, M. Schowalter, P. Venkata, S. Bley, C. Tessarek, D. Hommel, K. Sebald, M. Seyfried, J. Gutowski, A. Avramescu, K. Engl, and S. Lutgen, Ultramicroscopy **111**, 1316 (2011).

[32] S. S. Iyer, J. C. Tsang, M. W. Copel, P. R. Pukite, and R. M. Tromp, Appl. Phys. Lett. **54**, 219 (1989).

[33] P. C. Zalm, G. F. A. van de Walle, D. J. Gravesteijn, and A. A. van Gorkum, Appl. Phys. Lett. **55**, 2520 (1989).

[34] R. J. Jaccodine, J. Electrochem. Soc. **110**, 524 (1963).

[35] G. Radtke, M. Couillard, G. A. Botton, D. Zhu, and C. J. Humphreys, Appl. Phys. Lett. **97**, 251901 (2010).